Precipitation of MeV and Sub-MeV Electrons Due to Combined Effects of EMIC and ULF Waves

X. -J. Zhang, D. Mourenas, A. V. Artemyev, V. Angelopoulos, J. -A. Sauvaud

JGR Space Physics

RESEARCH ARTICLE
10.1029/2019JA026566

Precipitation of MeV and Sub-MeV Electrons Due to Combined Effects of EMIC and ULF Waves

X.-J. Zhang[1], D. Mourenas[2], A. V. Artemyev[1], V. Angelopoulos[1], and J.-A. Sauvaud[3]

[1]Institute of Geophysics and Planetary Physics, University of California, Los Angeles, CA, USA, [2]CEA, DAM, DIF, Arpajon, France, [3]Institut de Recherche en Astrophysique et Planetologie, Universite de Toulouse, CNRS, UPS, CNES, Toulouse, France

Key Points:
- Occurrence rates of simultaneous, intense EMIC and Pc4–Pc5 ULF waves in the outer radiation belt are provided
- The minimum energy of electrons precipitated by EMIC waves could theoretically decrease by 25% due to ULF waves
- We conjecture that EMIC waves could cause sub-MeV electron loss in the presence of intense Pc5 ULF waves near $L = 6$

Correspondence to:
X.-J. Zhang,
xjzhang@ucla.edu

Citation:
Zhang, X.-J., Mourenas, D., Artemyev, A. V., Angelopoulos, V., & Sauvaud, J.-A. (2019). Precipitation of MeV and sub-MeV electrons due to combined effects of EMIC and ULF waves. *Journal of Geophysical Research: Space Physics*, *124*, 7923–7935. https://doi.org/10.1029/2019JA026566

Received 28 JAN 2019
Accepted 8 AUG 2019
Accepted article online 7 SEP 2019
Published online 30 OCT 2019

Abstract We explore the mechanism of MeV and sub-MeV electron precipitations into the atmosphere in the outer radiation belt, through quasi-linear pitch-angle scattering by electromagnetic ion cyclotron (EMIC) waves, when strong compressional Pc4–Pc5 ultralow-frequency (ULF) waves are simultaneously present. Theoretically, the opposite magnetic field and density modulations produced by such ULF waves can significantly reduce the minimum electron energy for cyclotron resonance with EMIC waves, and this could potentially lead to the loss of lower energy (MeV and sub-MeV) electrons. Statistical satellite observations of simultaneous, intense EMIC and ULF waves reveal the parameter domains most conducive to such lower energy electron losses, which are shown to be mostly located near the geosynchronous orbit. Selected events further suggest that such a mechanism could be efficient in the outer radiation belt and that even larger effects might occur during strong injections from the plasma sheet.

1. Introduction

Dropouts of relativistic electrons are frequent in the outer radiation belt (Boynton et al., 2016, 2017; Green et al., 2004; Turner et al., 2012). Two different physical mechanisms have been proposed to explain them: magnetopause shadowing loss enhanced by the outward radial diffusion after a strong solar wind pressure pulse (Shprits et al., 2006; Turner et al., 2012) and precipitation into the atmosphere through pitch-angle scattering by electromagnetic ion cyclotron (EMIC) waves during disturbed periods (Blum et al., 2015; Bortnik et al., 2006; Hendry et al., 2017; Kersten et al., 2014; Mourenas et al., 2016; Sandanger et al., 2007; Summers & Thorne, 2003; Thorne & Kennel, 1971; Wang et al., 2014; Yu et al., 2015; Zhang et al., 2017). Since quasi-linear diffusion by EMIC waves alone cannot produce dropouts for all MeV electrons, due to a lack of cyclotron resonance at high equatorial pitch angles (Cao et al., 2017; Kersten et al., 2014; Ni et al., 2018; Usanova et al., 2014), a combined scattering by EMIC and chorus (e.g., Agapitov et al., 2018) waves present on the same L-shell has been invoked (Mourenas et al., 2016; Zhang et al., 2017). But this kind of dropout can only occur above the minimum energy, E_{min}, for cyclotron resonance with EMIC waves (Mourenas et al., 2016; Zhang et al., 2017). E_{min} is therefore a key parameter when trying to explain observations of either partial losses or full dropouts of MeV and sub-MeV electrons associated with EMIC waves.

Various studies have demonstrated that the minimum energy (E_{min}) for cyclotron resonance with hydrogen-band EMIC waves (left-hand polarized and quasi-parallel) is generally ≃1–3 MeV (Cao et al., 2017; Chen et al., 2011; Kersten et al., 2014; Mourenas et al., 2016; Ni et al., 2018; Summers & Thorne, 2003; Zhang et al., 2017), with low E_{min} corresponding to typical proton concentrations $\eta_p > 0.7$ (Kersten et al., 2014). Helium-band and oxygen-band EMIC waves usually lead to higher E_{min}, especially when taking into account hot plasma effects (Cao et al., 2017; Kersten et al., 2014; Ni et al., 2018; Summers & Thorne, 2003). However, electron precipitation associated with EMIC waves has often been observed down to smaller energies, ~0.4–1 MeV (Blum et al., 2015; Hendry et al., 2017; Wang et al., 2014; Zhang et al., 2017). Statistical studies of relativistic electron dropouts observed at $L \sim 4.2$ (where L denotes the McIlwain shell parameter) have also suggested the presence of EMIC wave-induced losses starting at low energies ~0.6–0.8 MeV (Boynton et al., 2016, 2017).

An open question, however, is how EMIC waves can contribute to electron losses at sub-MeV energies, that is, at significantly smaller energy than the minimum energy ($E_{min} > 1$–2 MeV) of cyclotron resonance with typical EMIC waves (Cao et al., 2017; Kersten et al., 2014; Mourenas et al., 2016; Ni et al., 2018; Summers &

Thorne, 2003; Zhang et al., 2017). Chen et al. (2016) have recently shown that intense (~1 nT) helium-band EMIC wave packets with sharp edges could produce such low-energy electron losses through nonresonant scattering. But this mechanism requires very sharp wave edges, less than several wavelengths between zero and the peak wave power, and EMIC wave frequencies close to the helium gyrofrequency, which may not be very frequent.

Using statistics of Van Allen Probes observations, Xiang et al. (2018) have recently found that the minimum energy of electron dropouts varies with equatorial pitch angle α_0 roughly like the theoretically expected $E_{\min}(\alpha_0)$ for cyclotron resonance with hydrogen-band EMIC waves (Cao et al., 2017; Kersten et al., 2014; Mourenas et al., 2016; Ni et al., 2018; Zhang et al., 2017) at $L^* \leq 4$ (L^* is the adiabatically invariant L-shell) but that it decreases below $E_{\min}(\alpha_0)$ at $L^* = 5$. This indicates that low-energy electron losses related to EMIC waves are mainly localized at high $L^* \geq 5$. Another recent statistical study has found that simultaneous intense Pc5 ultralow-frequency (ULF) waves at 1–10 mHz and EMIC waves at 0.5–5 Hz can produce stronger ~0.7- to 2-MeV electron losses than EMIC waves alone, suggesting a possible synergistic effect of EMIC and ULF waves (Simms et al., 2018). Such ULF waves may be excited by the solar wind through Kelvin-Helmholtz instability or dynamic pressure variations or internally via resonance with injected particles, reaching larger amplitudes at higher L (e.g., see ; Chen & Hasegawa, 1991; Kepko & Spence, 2003; Kivelson & Southwood, 1986; Mathie & Mann, 2001; Menk, 2011). The results from Simms et al. (2018) seem to imply that ULF waves could decrease $E_{\min}$. The possibility that ULF waves could affect $E_{\min}$ will be investigated in the present paper.

In the next section, we provide statistics of simultaneous observations of intense EMIC and ULF waves in the outer radiation belt, based on data from the Van Allen Probes and Time History of Events and Macroscale Interactions during Substorms (THEMIS) mission. Then, we discuss analytical estimates of the minimum energy ($E_{\min}$) of electron loss in the presence of ULF and EMIC waves. We show that realistic, intense compressional Pc4–Pc5 ULF waves can indeed reduce $E_{\min}$ for cyclotron resonance with EMIC waves at high $L \simeq 5.5$–6.6, enabling hydrogen-band EMIC waves (without sharp edges) to precipitate electrons at low energies unattainable without ULF waves. Finally, selected conjugate observations of simultaneous EMIC and ULF waves near the equator and electron precipitations at low altitude are examined. They suggest that the proposed mechanism may be operating in the outer radiation belt.

2. Relativistic Electron Loss in the Presence of EMIC and ULF Waves

For the sake of simplicity, we consider plasma and hydrogen-band EMIC wave parameters such that $\omega_{\rm EMIC}/\Omega_{cp0} > 0.85 - \eta_p/2$, with $\omega_{\rm EMIC}$ the EMIC wave frequency, $\Omega_{\rm cp0}$ the proton equatorial gyrofrequency, and $\eta_p \simeq 0.9$–1.0 as usual during hydrogen-band EMIC wave observations (Kersten et al., 2014). For such conditions, the full dispersion relation of nearly parallel hydrogen-band EMIC waves (Summers & Thorne, 2003) can be simplified, giving a minimum resonant energy (see Mourenas et al., 2016)

$$E_{\min}[\mathrm{MeV}] \approx \frac{\sqrt{1+K}-1}{2} \quad \text{with} \quad K = \frac{\Omega_{\rm ce0}^2}{\Omega_{\rm pe0}^2 \cos^2\alpha_0} \frac{\Omega_{\rm cp0}^2 (1-\omega_{\rm EMIC}/\Omega_{\rm cp0})(m_{\rm p}/m_{\rm e})}{\omega_{\rm EMIC}^2 (1-\Omega_{\rm cp0}(1-\eta_p)/\omega_{\rm EMIC})}, \tag{1}$$

with $\Omega_{\rm ce0}$ and $\Omega_{\rm pe0}$ the electron equatorial cyclotron and plasma frequencies, α_0 its equatorial pitch angle, and $m_{\rm e}$ and $m_{\rm p}$ the electron and proton masses. Since we hereafter investigate the effects of EMIC waves on electrons over timescales of hours and, therefore, integrated over MLT (magnetic local time), we consider a fixed range of normalized EMIC wave frequencies within $\omega_{\rm EMIC}/\Omega_{\rm cp0} \simeq 0.35$–$0.65$. This frequency range is consistent with typical time- and MLT-averaged spectra of intense hydrogen-band EMIC waves (Meredith et al., 2014; Zhang et al., 2016, 2017). A crucial point here is that compressional Pc4–Pc5 ULF waves recorded in the inner magnetosphere often produce comparable but opposite variations of magnetic pressure ($\sim \Delta B^2/B^2$) and plasma pressure or density ($\sim \Delta N_{\rm e}/N_{\rm e}$) to maintain the local pressure equilibrium (Chen & Hasegawa, 1991; Li et al., 2011; Li et al., 2017; Xia et al., 2016). Such B and $N_{\rm e}$ variations due to ULF waves combine constructively in the term K in equation (1), which varies as $\Omega_{\rm ce0}^2/\Omega_{\rm pe0}^2$, that is, like $B^2/N_{\rm e}$. Statistics of Pc4–Pc5 ULF waves have shown mean variations of $\Delta B \sim 30$ nT in the outer radiation belt during geomagnetic storms when $Kp = 4-7$, sometimes reaching more than 50 nT near $L = 6$ (Mathie & Mann, 2001; Murphy et al., 2016; Potapov et al., 2006). Significant $\Delta B/B \approx 0.1 - 0.5$ levels are not uncommon at

geosynchronous orbit (Rae et al., 2018). Plasma density variations $\Delta N_e/N_e$ are often found to be opposite in phase and of the same order as $\Delta B^2/B^2$, although occasionally reaching levels of 10 times larger (Li et al., 2011; Li et al., 2017; Xia et al., 2016).

Equation (1) shows that the minimum energy (E_{min}) for cyclotron resonance with EMIC waves decreases when $K \propto \Omega_{ce0}^2/\Omega_{pe0}^2$ decreases. This means that intense compressional ULF waves can possibly reduce E_{min} during half of the ULF wave period—when B is diminished and N_e is increased. Since the quasi-static geomagnetic field B is already reduced during strong storms at $L > 5$ on the nightside, this region could potentially be more propitious for a strong decrease of B due to ULF waves and a strong synergistic effect of ULF and EMIC waves on low-energy electron precipitation. In addition, smaller B^2/N_e, denser injected hot proton populations, and stronger proton temperature anisotropy lead to higher EMIC wave growth rates and higher normalized frequencies (Chen et al., 2011; Remya et al., 2018). As a result, Pc5 ULF waves can modulate EMIC wave growth, probably accounting for some EMIC wave intensity modulations at Pc5 frequencies observed in space (e.g., see Mursula et al., 2001; Menk, 2011).

In the present study, we use EMIC and ULF wave measurements from the magnetometer of the Electric and Magnetic Field Instrument Suite and Integrated Science (EMFISIS) payload (Kletzing et al., 2013) onboard the Van Allen Probes (Mauk et al., 2013) at $L \leq 6$ and similar wave measurements from the fluxgate magnetometer (Auster et al., 2008) of THEMIS spacecraft that cover higher L-shells (Angelopoulos, 2008). For the Van Allen Probes data set, the plasma density is calculated from the upper hybrid resonance frequency (Kurth et al., 2015) measured by the Electric and Magnetic Field Instrument Suite and Integrated Science High-Frequency Receiver or from the spacecraft potential measured by the Electric Field and Waves instrument (Wygant et al., 2013). For the THEMIS data set, the plasma density is inferred from the spacecraft potential measurements (Bonnell et al., 2008). We take into account only well-defined compressional Pc4–Pc5 ULF waves observed at a given L-shell in the 5–100 mHz range by one THEMIS spacecraft or in the 10–100 mHz range by one Van Allen Probe, by imposing the following three requirements: (i) continuous availability of ULF wave measurements over a time period of <20 min centered on the EMIC wave observation, corresponding to a variation of the spacecraft position smaller than 0.5 Earth radius, (ii) availability of measurements over at least several ULF wave periods to get well-defined waves, and (iii) presence of periodical density fluctuations in opposite phase to magnetic ULF fluctuations. The limit of <20 min on the observation time, together with the requirement of observing at least several ULF wave periods, leads to a relatively high minimum ULF frequency, ~5–10 mHz. This strict selection procedure can underestimate the total ULF wave power in the Pc4–Pc5 range, because ULF wave power is often stronger at lower frequencies and because weaker ULF waves may be simultaneously present at different frequencies. Consequently, it is important to keep in mind that the statistical ULF wave intensities provided below are very conservative values. Using the above criteria forTHEMIS (in 2007–2011) and Van Allen Probes (in 2012–2015) data, we have found 31 events (simultaneous observations of hydrogen-band EMIC waves and intense Pc5 ULF waves) from THEMIS in the L-shell range of 6.0–7.0, 83 events from the Van Allen Probes in the L-shell range of 5.5–6.0, and 53 events from the Van Allen Probes in the L-shell range of 4.0–5.5.

Figures 1a–1d display the distribution of simultaneous observations (captured by Van Allen Probes or THEMIS) of hydrogen-band EMIC waves and intense ($\Delta B/B > 0.005$) Pc5 ULF waves at $L = 5.5$–7.0 as a function of MLT, maximum $\Omega_{pe0}/\Omega_{ce0}$ ratio (inferred from local plasma density and geomagnetic field measurements), ULF wave magnetic field variations ($\Delta B/B$) and density variations ($\Delta N_e/N_e$), the corresponding $(\Delta N_e/N_e)/(\Delta B^2/B^2)$ ratio, and maximum normalized EMIC wave frequency $\max(\omega_{EMIC}/\Omega_{cp0})$. Hydrogen-band EMIC waves with high frequencies $\max(\omega_{EMIC}/\Omega_{cp0}) \geq 0.55$–$0.60$ are often found in the dusk sector when $\Omega_{pe0}/\Omega_{ce0} \sim 18$–$27$ (see Figures 1a and 1d). During periods with $\Omega_{pe0}/\Omega_{ce0} \sim 18$–$27$, EMIC waves are mainly observed together with intense compressional ULF waves such that $(\Delta N_e/N_e)/(\Delta B^2/B^2) \sim 1$–$3$ (see Figure 1c), mainly corresponding to $\Delta B/B \sim 0.012 - 0.10$ in Figure 1b. We shall demonstrate below that the simultaneous presence of such EMIC and ULF waves in high-density regions can lead to lower E_{min} levels than if EMIC waves were observed alone.

Figures 1e and 1f show the occurrence rate and the weighted (by ULF wave intensity) occurrence rate of coincident observations of hydrogen-band EMIC waves and ULF waves. The occurrence rate of simultaneous ULF and EMIC wave observations is about 0.1% in general at a given L-shell. Based on the present Van Allen Probes statistics and CRRES statistics of hydrogen-band EMIC wave occurrences (Meredith et al., 2014; Zhang et al., 2016), it means that ULF waves are probably present roughly 10% of the time when intense

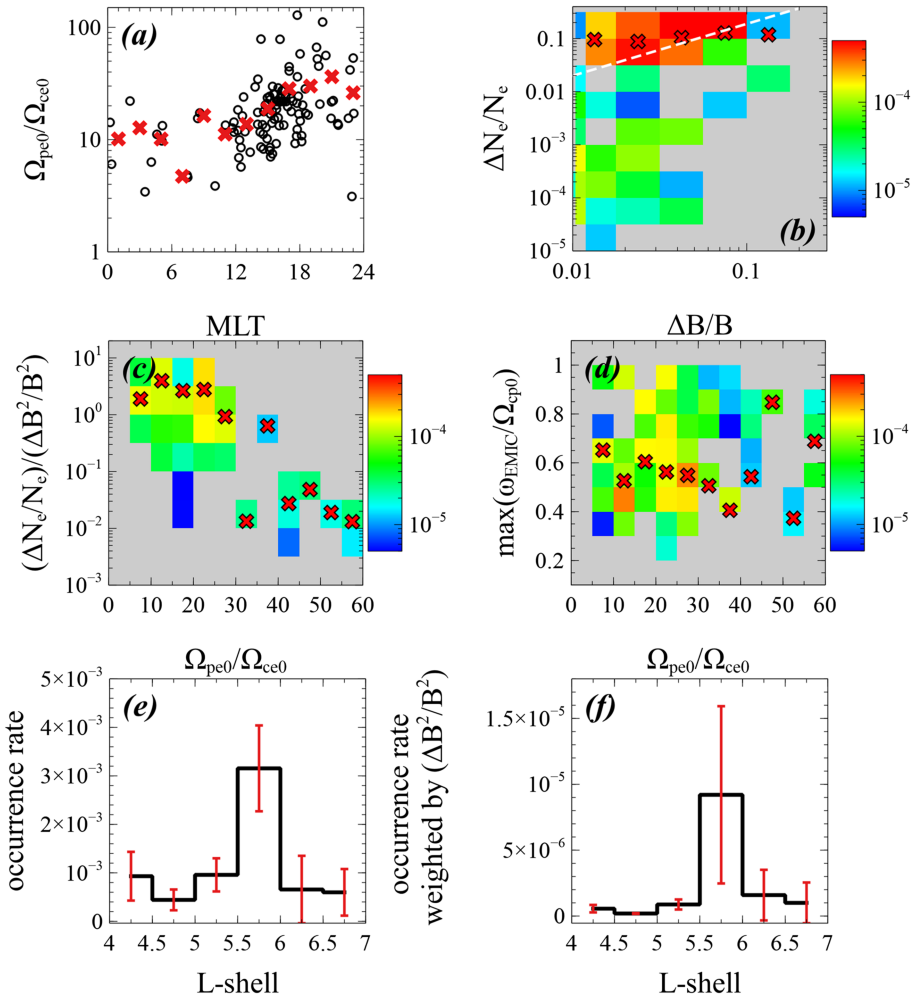

Figure 1. (a) Measured $\Omega_{pe0}/\Omega_{ce0}$ ratio (black points) during simultaneous observations of hydrogen-band electromagnetic ion cyclotron (EMIC) waves (with amplitudes >0.1 nT for the Van Allen Probes and >0.05 nT for THEMIS) and intense ($\Delta B/B > 0.005$) Pc5 ultralow-frequency (ULF) waves at $L = 5.5–7.0$, captured by Van Allen Probes (in 2012–2015) or THEMIS (in 2007–2011), as a function of MLT. The mean $\Omega_{pe0}/\Omega_{ce0}$ in each MLT bin are shown by red crosses. (b) Distribution of the same events as in (a), as a function of maximum $\Delta B/B$ and of the corresponding (opposite in phase) maximum $\Delta N_e/N_e$. The dotted white line marks the ratio $\Delta = (\Delta N_e/N_e)/(\Delta B^2/B^2) = 1$. Mean $\Delta N_e/N_e$ values in $\Delta B/B$ bins are shown by red crosses. (c) Distribution of the same events as a function of $\Delta = (\Delta N_e/N_e)/(\Delta B^2/B^2)$ ratio and the maximum measured $\Omega_{pe0}/\Omega_{ce0}$. Mean Δ values are shown by red crosses in $\Omega_{pe0}/\Omega_{ce0}$ bins. (d) Distribution of the same events, as a function of the maximum normalized EMIC wave frequency $\max(\omega_{EMIC}/\Omega_{cp0})$ and the measured $\Omega_{pe0}/\Omega_{ce0}$. Red crosses show mean $\max(\omega_{EMIC}/\Omega_{cp0})$ values in $\Omega_{pe0}/\Omega_{ce0}$ bins. (e) Distribution of occurrences of simultaneous hydrogen-band EMIC and ULF wave observations (with error bars in each L-shell bin) as a function of L-shell, based on THEMIS and Van Allen Probes statistics and calculated as the ratio of times of combined EMIC and ULF wave observations to the total time of spacecraft observations in a given L bin. Only strong ULF waves with $\Delta B/B > 0.005$ and EMIC waves with amplitudes > 0.1 nT are considered. (f) Same as (e) for the distribution of occurrences weighted by ULF wave intensity, $(\Delta B^2/B^2)$.

(amplitudes > 0.1 nT) hydrogen EMIC waves are present. Both the occurrence rate and the weighted (by ULF wave intensity) occurrence rate strongly increase as L increases from 4.0–5.5 to 5.5–6.0, respectively, by factors ~3 and ~10. This suggests a much stronger statistical impact of ULF waves on EMIC-driven electron precipitation at $L \sim 5.5–6.0$. Such a stronger presence of intense compressional ULF waves together with EMIC waves at $L \geq 5.5$ might also account for the decrease of the minimum energy of electron dropouts below the theoretical threshold for EMIC waves alone, observed at $L^* = 5$ but not at lower $L^* \leq 4.5$ (Xiang et al., 2018).

Figure 1a shows that events with high $\Omega_{pe0}/\Omega_{ce0}$, leading to lower E_{min} values, are more abundant on the nightside and near dusk, probably in association with high-density plasma plumes, strong ion injections,

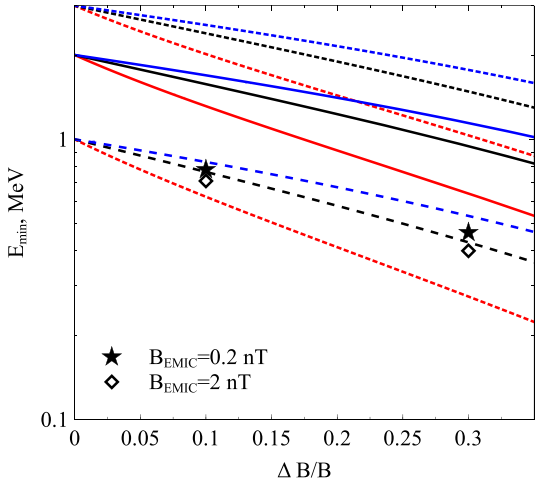

Figure 2. Minimum electron resonant energies, E_{min}, from equation (1) for cyclotron resonance with parallel left-hand hydrogen-band electromagnetic ion cyclotron (EMIC) waves in the simultaneous presence of intense compressional ultralow-frequency (ULF) waves, displayed as a function of $\Delta B/B = 0$–0.3 for different levels of $\Delta = (\Delta N_e/N_e)/(\Delta B^2/B^2) = 1, 3, 5$ (shown in blue, black, and red, respectively), when $E_{min} = 1, 2$, or 3 MeV (shown by dashed, solid, and dotted curves, respectively) without ULF waves. Minimum electron energies, E_{min}, obtained numerically from test-particle simulations in the simultaneous presence of EMIC waves and intense ULF waves at 1.5 mHz, are shown by black stars and triangles, respectively, for $E_{min}(\Delta B = 0) = 1$ MeV and mean EMIC wave amplitudes of 0.2 and 2 nT (the EMIC wave amplitude increases from 0.5 to 1.5 times its mean value over $\lambda = 0$–10°).

or magnetic field line stretching during storms (Remya et al., 2018). The distribution of these events as a function of the maximum measured $\Delta B/B$ and of the opposite-in-phase maximum $\Delta N_e/N_e$ is displayed in Figure 1b.

Equation (1) can be rewritten as $4(E_{min}^2 + E_{min}) = K$. Assuming a fixed and finite value of $\Delta = (\Delta N_e/N_e)/(\Delta B^2/B^2)$ for ULF waves and considering the ratio $K(\Delta B)/K(\Delta B = 0)$ yields a quadratic equation $E_{min}^2(\Delta B) + E_{min}(\Delta B) - [K(\Delta B)/K(\Delta B = 0)][E_{min}(\Delta B = 0)^2 + E_{min}(\Delta B = 0)] = 0$ for $E_{min}(\Delta B)$. In this equation, the term $K(\Delta B)/K(\Delta B = 0)$ depends only on $\Delta B/B$ and $\Delta N_e/N_e$—it is independent of wave $(\omega_{EMIC}/\Omega_{cp0})$ and plasma $(\eta_p, \Omega_{pe0}/\Omega_{ce0})$ parameters (and α_0) for fixed values of $\omega_{EMIC}/\Omega_{cp0}$ and η_p assumed independent of ΔB. Therefore, the above equation provides $E_{min}(\Delta B)$ as a function of $E_{min}(\Delta B = 0)$ whatever the wave and plasma parameters. This allows us to plot $E_{min}(\Delta B)$ (in the presence of ULF waves) as a function of $(\Delta B/B)$ in Figure 2, demonstrating that E_{min} can be strongly reduced by intense Pc5 ULF waves. These results agree with test-particle simulations performed for moderate EMIC wave amplitudes (0.2 nT).

For typical compressional ULF waves amplitudes, $\Delta B/B \sim 0.05$–0.15, shown in Figures 1b and 1c, and usual levels of $(\Delta N_e/N_e)/(\Delta B^2/B^2) \sim 1$–5 at $L \sim 6$, the minimum electron energy (E_{min}) for cyclotron resonance with EMIC waves can be decreased by 20–30%. For higher ULF wave amplitudes, ~20–30 nT, recorded during storms, corresponding to $\Delta B/B \sim 0.2$–0.3 at $L \sim 6$, one can even get an ~50% decrease in E_{min}, sufficient to reach 0.5–0.7 MeV.

Results of test-particle simulations (Albert & Bortnik, 2009; Su et al., 2012; Wang et al., 2017) performed with hydrogen-band EMIC waves of very high amplitude, ~2 nT (Meredith et al., 2014), in the presence of modulations of B and N_e induced by ULF waves are also given in Figure 2. For such high EMIC wave amplitudes, the resonance width is determined by wave amplitude (e.g., see ; Artemyev et al., 2014; Omura & Zhao, 2013, and references therein), and an increase of the resonance width with wave amplitude further reduces E_{min} by 10–15% for realistic amplitudes of ~2 nT as compared with weaker average amplitudes of 0.2 nT.

The maximum equatorial pitch angle $\alpha_{0,max}$(EMIC) of electrons at energy E that can reach cyclotron resonance with EMIC waves is given by $\cos^2\alpha_{0,max}(\text{EMIC}) = (E_{min}^2 + E_{min})/(E^2 + E)$, which is proportional to B^2/N_e in the EMIC wave region (Mourenas et al., 2016). $\alpha_{0,max}$(EMIC) remains < 50° for $E < (1.6-2.0)\times E_{min}$. Therefore, additional pitch-angle diffusion by whistler-mode chorus or hiss waves is generally required at higher equatorial pitch angles to scatter all MeV electrons toward the loss cone and induce a strong dropout (Mourenas et al., 2016, 2017; Zhang et al., 2017):

3. Selected Observations of Relativistic Electron Loss in the Presence of EMIC and ULF Waves

Figure 3 shows two events with simultaneous intense EMIC and ULF waves, accompanied by signatures of electron precipitation. Panels (a)–(d) show the first event containing (a) EMIC waves in the hydrogen band measured by the magnetometer (Kletzing et al., 2013) onboard the Van Allen probes at $L \sim 5.5$, (b) ULF waves measured by GOES at a slightly higher L (~6.6) than EMIC waves but such that the typical radial scale (~1–2 R_E) of ULF waves still encompasses the EMIC wave region (Degeling et al., 2008; Hartinger et al., 2013), and (c) precipitating electron fluxes measured by POES. Corresponding spacecraft trajectories in the (MLT, L-shell) space are shown in Figure 3d. Since accurate Pc5 ULF wave measurements require prolonged observations at an almost fixed L and the orbit of Van Allen Probes generally does not allow such fixed L measurements, we use measurements from GOES at geostationary orbit, in an (MLT, L-shell) sector sufficiently close to Van Allen Probes observations (see Figure 3d). The intense hydrogen-band EMIC waves reach frequencies of $\omega_{\mathrm{EMIC}}/\Omega_{\mathrm{cp}} \sim 0.5$ on different occasions between 11:02 UT and 11:10 UT, allowing them to interact resonantly with electrons of lower energy (Kersten et al., 2014). During the conjugate observations between Van Allen Probes and POES, significant and sporadic increases of precipitating (field-aligned) electron fluxes measured by POES can be seen in Figure 3c after 11:02 UT in the ≈300- to 700-keV energy range, sometimes reaching the level of the trapped fluxes (at 90°). Such sub-MeV electrons could have been affected by resonant wave-particle interactions and precipitated into the atmosphere, possibly by the combined effects of EMIC and ULF waves (see similar observations from Capannolo et al., 2018). Simultaneously with EMIC wave observations, some decrease of field-aligned electron (0.5–1.5 MeV) fluxes was observed by the Van Allen Probes near the equator (not shown): It could also be due to a precipitation induced by EMIC waves (e.g., see Usanova et al., 2014; Wang et al., 2014). However, there is also an increase of precipitating fluxes at lower energies ~30–100 keV, suggesting that part of the observed precipitation during this event might simply be due to the widening of the loss cone caused by the same ULF waves (Rae et al., 2018).

Figures 3e–3h show a second event with simultaneous EMIC and ULF wave observations by THEMIS spacecraft (Angelopoulos et al., 2008) and electron precipitation measured by the low-altitude DEMETER satellite (Parrot et al., 2006). The DEMETER-THEMIS conjugation time is indicated by a vertical line in Figures 3e and 3f. It corresponds to interspacecraft separations of ~0.4 in L and ~0.6 hr in MLT– smaller than typical scales of hydrogen-band EMIC waves and ULF waves (Blum et al., 2017; Degeling et al., 2008; Hartinger et al., 2013; Lee et al., 2013). The THEMIS magnetometer (Auster et al., 2008) detected hydrogen-band EMIC waves (extending up to $\omega_{\mathrm{EMIC}}/\Omega_{\mathrm{cp}} \sim 0.45$) and compressional ULF waves (note that the magnetic field intensity seen below the oxygen cyclotron frequency in Panel (e) actually corresponds to the spectrum of the compressional ULF waves shown in Panel (f)). During the THEMIS/DEMETER conjugation, the Instrument of Detection of Particles onboard DEMETER (Sauvaud et al., 2006) collected the electron spectrum (Figure 3g). Due to the Instrument of Detection of Particles viewing angle, this spectrum mostly corresponds to trapped particles. Therefore, we compare it with two spectra measured at the same MLT and L-shell during DEMETER orbits just before and after the conjugation event (as in previous studies; e.g., see Hendry et al., 2017). In Figure 3g, the electron spectrum collected during the conjugation event has a lower level (by a factor of 3 to 5) of high-energy (400–1,000 keV) particles, as compared with the preceding and following orbits. This could be related to a precipitation driven by electron interaction with EMIC waves in the presence of ULF waves. The observed precipitation loss, absent below 350 keV and increasing with energy above 400 keV, seems unlikely to have been produced by the sole ULF wave-induced loss-cone widening (Rae et al., 2018), which should generally lead to similar losses at all energies.

For the two events in Figure 3, calculations of E_{min} show that the extension of EMIC wave-induced precipitation to such low energies by simultaneous ULF waves would require ~5–10 times larger ULF wave amplitudes (in the EMIC wave region at $L \simeq 5.2$–5.5) than recorded by THEMIS at $L = 5.2$ or by GOES at $L = 6.6$. However, as noted above, such Pc4–Pc5 ULF waves could not be measured accurately by THEMIS. Accordingly, their actual amplitudes in the EMIC wave-electron interaction region remains unknown in both cases and could have been much larger than in Figures 3b and 3f. Rae et al. (2018) have indeed revealed the presence of at least five compressional ULF wave events per week at $L = 6.6$, with ULF waves reaching median amplitudes of ≈30–40 nT. Ozeke et al. (2014) have further shown that compressional ULF wave power at $L \simeq 5.2$ is generally half of that at $L \simeq 6.6$. Consequently, the needed ULF waves with peak amplitudes of ~10–15 nT could really have been present in the EMIC wave region during these two events

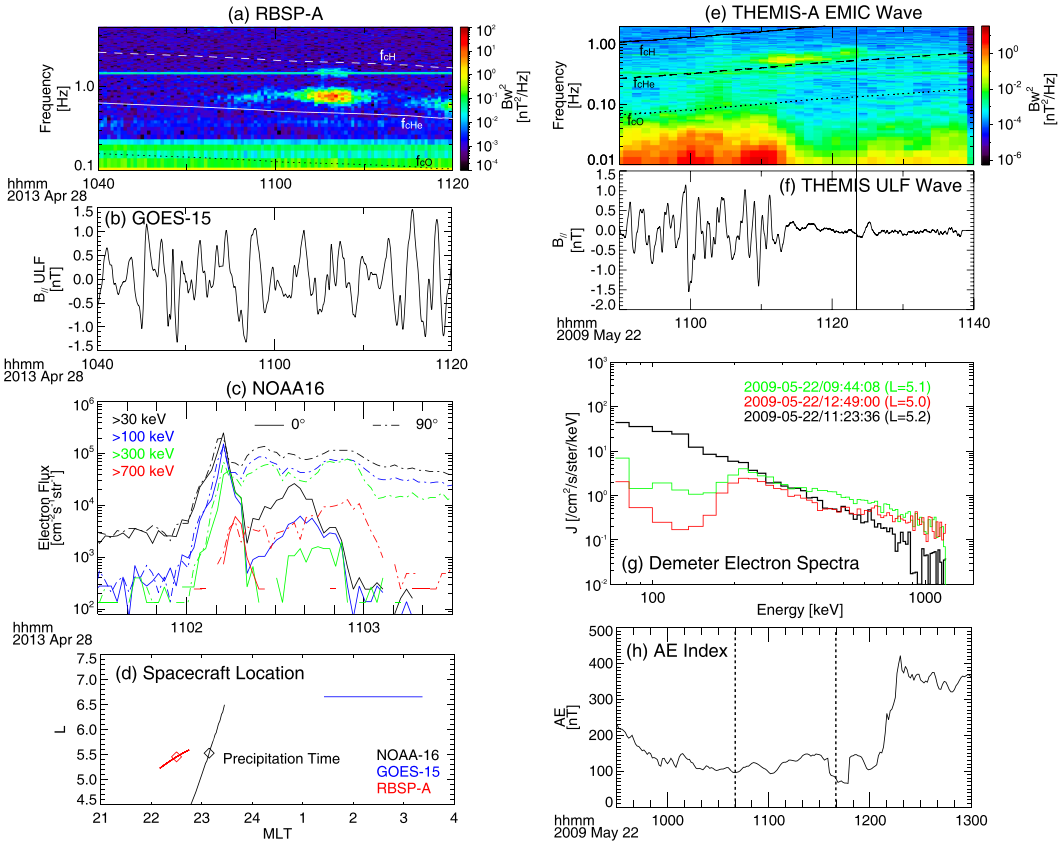

Figure 3. Two events of simultaneous observations of electromagnetic ion cyclotron (EMIC) waves, ultralow-frequency (ULF) waves, and electron precipitations: (a)–(d) show an event on 28 April 2013, and (e)–(h) show an event on 22 May 2009. (a) EMIC waves observed by the Van Allen Probes (dashed, solid, and dotted lines show proton, helium, and oxygen gyrofrequencies, respectively); (b) compressional ULF wave observed by GOES 15; (c) precipitating and trapped electron fluxes observed by POES 16; (d) spacecraft trajectories in the (MLT, *L*-shell) space; (e, f) EMIC (dashed, solid, and dotted lines show proton, helium, and oxygen gyrofrequencies, respectively) and ULF waves observed by Time History of Events and Macroscale Interactions during Substorms (THEMIS) A with the same time axis; the vertical line shows the time of THEMIS conjugation with DEMETER; (g) trapped electron spectra observed by DEMETER during conjugation with THEMIS (black curve), as well as one orbit before and after this conjugation (green and red curves); (h) AE index over the time interval including three DEMETER orbits (for reference, dotted vertical lines mark the interval in (e) and (f)).

(possibly slightly away from THEMIS orbit in the second case). These two events are therefore nice potential cases of EMIC and ULF wave-induced precipitation, although they cannot be considered as the definitive evidence. The entire interval of the second event on May 2009, including the first two DEMETER orbits, is characterized by a low AE index (see Figure 3h) with neither strong injection nor magnetic field reconfiguration that could have affected electron spectra measured by DEMETER. However, the third DEMETER orbit is accompanied by substorm activity with $AE > 300$ nT: Some of the differences between the first and last DEMETER spectra could be due to the magnetic field reconfiguration during the third orbit.

ULF wave amplitudes shown in Figures 3b and 3f do not reach the high levels (~25–35%) of the background magnetic field reported by Rae et al. (2018) during many events. Conjugate observations of such intense ULF waves and electron precipitation by GOES or THEMIS can be found, but the majority of such strong ULF wave observations are accompanied by strong plasma injections with rapid changes of particle fluxes and magnetic field configuration. During injections (accompanied by current sheet thinning and the following dipolarization; see, e.g., Runov et al., 2009, and references therein), finding accurate POES conjugations with equatorial measurements (from GOES or Van Allen Probes) is problematic due to the strongly varying magnetic field configuration: The results of such conjugate observations should be taken with caution.

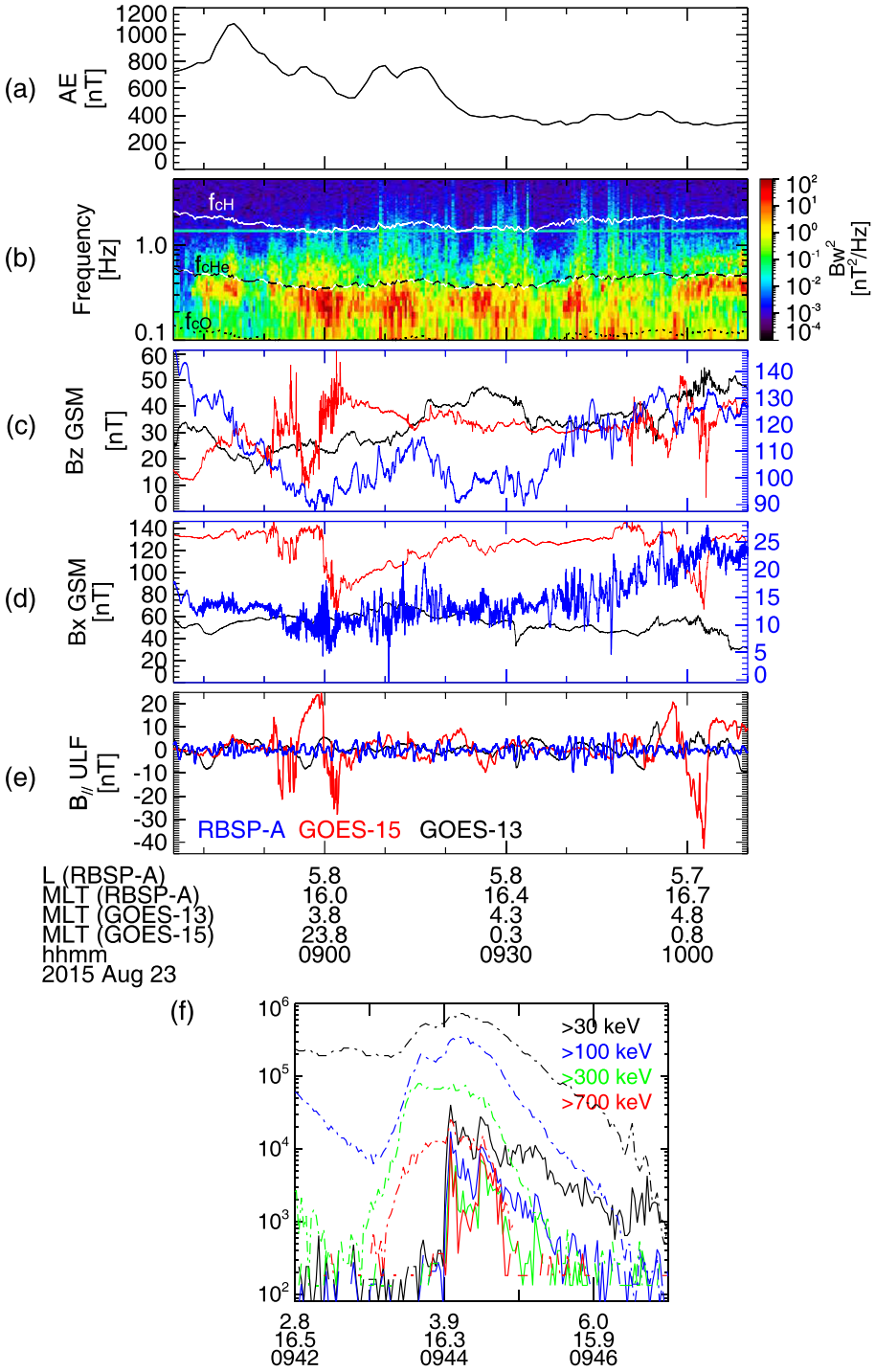

Figure 4. An exemplifying 1-hr interval of increased geomagnetic activity: (a) *AE* index; (b) electromagnetic ion cyclotron waves captured by the Van Allen Probe A (RBSP-A); (c, d) magnetic field measured by GOES 13 and 15 (left axes) and the Van Allen Probe A (right axes); (e) compressional magnetic field fluctuations in the ultralow-frequency (ULF) range; (f and g) POES observations of precipitating and trapped electron fluxes.

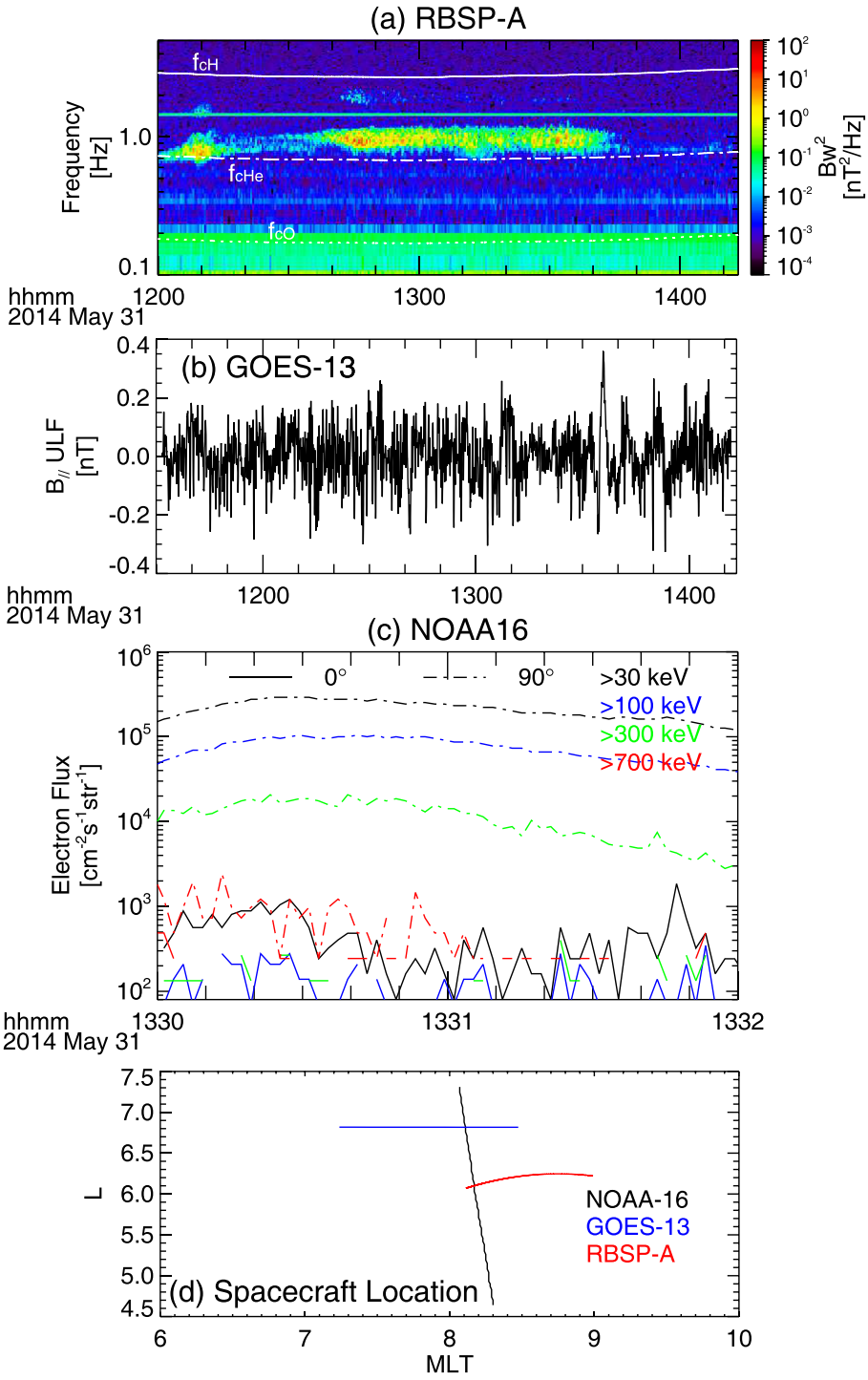

Figure 5. An example of electromagnetic ion cyclotron wave observations conjugated with no precipitation of low-energy electron fluxes; (a) electromagnetic ion cyclotron waves captured by the Van Allen Probe A (RBSP-A); (b) compressional magnetic field fluctuations in the ultralow-frequency (ULF) range; (c) POES observations of precipitating and trapped electron fluxes; (d) spacecraft trajectories in the (MLT, *L*-shell) space.

One such event is shown in Figure 4. This 2-hr time interval is characterized by an elevated *AE* index (>400 nT) and a series of plasma injections. The near-midnight magnetic field measured by GOES 15 shows several strong B_z perturbations (dipolarizations) preceded by $|B_x|$ increase (current sheet thinning). Similar B_z perturbations are observed by GOES 13 (see Figures 4c and 4d). The low-frequency compressional part of these perturbations can be considered as intense ULF waves (see Figure 4e), reaching ~50% of the background field. However, such perturbations contain rapid B_z changes around the injection front (the so-called dipolarization front; see Runov et al., 2009), which differs significantly from usual ULF waves. These intense injections continuously transport hot plasma sheet ions into the inner magnetosphere, where this anisotropic population often generates EMIC waves. During this entire 2-hr interval, the Van Allen Probes observed EMIC waves in the helium and hydrogen bands near dusk (see Figure 4b). POES crossed this MLT sector two times, each time observing a rapid increase of precipitating electron (>0.7 MeV) flux (at 08:04:20 and 09:44 UT). We cannot ascertain the conjugation of POES (around $L \sim 4$–4.5) and Van Allen Probes (near $L \sim 5.5$-6) observations during this event. Nevertheless, the existing stretched geomagnetic field line configuration (i.e., the increased $|B_x|$ observed by GOES) suggests that POES is likely at a significantly higher *L*-shell (closer to $L \approx 5.5$–6) than estimated in a dipolar magnetic field. Unfortunately, the adiabatically invariant shell parameter L^* evaluated using empirical magnetic field models does not allow to evaluate this effect, because such magnetic field models are not parameterized by *AE* and do not yet take into account substorm-/injection-driven magnetic field changes.

The event shown in Figure 4 suggests that the effect of ULF waves on electron precipitations induced by EMIC waves could become much stronger during disturbed times. Plasma injections can enhance ULF wave activity (Runov et al., 2014) and simultaneously provide the free energy for EMIC wave generation. Based on the simple estimates provided in section 2 for ordinary ULF waves, such large magnetic fluctuations could potentially lead to a reduction of the minimum energy $E_{\min}$ of electrons that can be precipitated via resonant interactions with EMIC waves down to ~0.25 to 0.5 times the usual (i.e., without ULF waves) $E_{\min}$. However, such strong injections modify the geomagnetic field topology, seriously complicating the interpretation of electron precipitation recorded by satellites at low altitudes. During important geomagnetic storms with $Dst < -100$ nT, the steady magnetic field strength can also be strongly reduced near local midnight at $L > 5$, lowering $E_{\min}$ when EMIC waves are present in this sector (Kang et al., 2015).

To demonstrate the potential importance of ULF wave effects on electron precipitation by EMIC waves, we finally compare the events shown in Figure 3 with another, similar event of EMIC wave observations at similar normalized frequencies and with similar amplitudes but this time without significant ULF waves. Figure 5 shows the Van Allen Probe (RBSP-A) observations of hydrogen-band EMIC waves, without any significant conjugated increase of precipitating fluxes of less than 1-MeV electrons, in stark contrast with the two events in Figure 3. No significant compressional ULF waves were detected during this period, allowing EMIC waves to scatter only high-energy (>1–2 MeV) electrons, without affecting lower energy electron fluxes.

4. Discussion and Conclusions

In this paper, we provided statistics of simultaneous observations of intense EMIC and compressional 5–100 mHz ULF waves in the outer radiation belt, based on measurements from Van Allen Probes and THEMIS. We have shown theoretically that realistic compressional ULF waves, with $\Delta B/B \sim 10\%$, relatively frequent in this region, could significantly reduce the minimum energy $E_{\min}$ for cyclotron resonance with hydrogen-band EMIC waves at $L \simeq 5.5$–6. This would allow for EMIC wave-induced electron precipitation at energies at least 20–30% smaller than without ULF waves.

We found a strong peak in the weighted (by ULF wave intensity) occurrence rate of such simultaneous EMIC and ULF wave observations at $L \simeq 5.5$–6.0. We conjecture that such a strong peak could potentially lead to a much stronger impact of ULF waves on EMIC-driven electron precipitation at these *L*-shells. It could partially explain the electron losses observed at energies below the theoretical threshold $E_{\min}$ for EMIC waves alone (Xiang et al., 2018). The same effect could also account for a statistical increase of ~0.7–2 MeV electron losses when both EMIC and ULF waves are present, as compared with EMIC waves alone (Simms et al., 2018).

We examined several events with simultaneous EMIC and ULF wave observations near the equator (captured by Van Allen Probes and GOES) and conjugate sub-MeV electron precipitation at low altitude

(recorded by POES or DEMETER). The existence of such observations partially supports our speculation that the proposed mechanism of ULF wave influence on EMIC wave-driven electron loss could be operating in the outer radiation belt. Such a mechanism could account for some observations of electron losses at lower energies (sub-MeV) than the threshold energy E_{min} for cyclotron resonance with EMIC waves alone. We caution, however, that such events only show that EMIC and ULF waves can be simultaneously present with electron precipitation at low energies but do not provide definitive evidence for the presence of this effect. A real proof for the effect of ULF waves on E_{min} would require events during which ULF waves are turned on and off while EMIC waves remain unchanged, with low-energy electron precipitation occurring only when ULF waves are present. No such event has yet been found, although we showed one event with similar EMIC waves but much weaker ULF waves, which did not lead to any measurable low-energy electron precipitation.

One additional event, occurring during successive injections from the plasma sheet, suggests that the associated complex and strong (~50%) decreases of the background magnetic field, in the dusk sector near $L = 6$, could produce even stronger effects on EMIC wave-induced electron loss than usual Pc5 ULF waves. Such injections also provide significant amounts of hot, anisotropic plasma sheet ions that can generate intense EMIC waves. A previous statistical study (Rae et al., 2018) has shown that such strong magnetic field fluctuations are frequent during disturbed periods at geosynchronous orbit. Based on simple estimates provided in this paper for usual ULF waves, such large magnetic fluctuations could lead to a significant reduction (by ~50–70%) of the minimum energy of electrons that can be resonantly scattered by EMIC waves. However, more work is needed to accurately estimate the effects of magnetic fluctuations on EMIC wave-electron interaction during such highly dynamical periods.

Acknowledgments
X. J. Z. and A. V. A. acknowledge the support of NASA Grant 80NSSC18K1112 and NASA Contract NAS5-02099 for use of data from the THEMIS Mission, specifically J. W. Bonnell and F. S. Mozer for use of EFI data, A. Roux and O. LeContel for use of SCM data, and K. H.Glassmeier, U. Auster, and W. Baumjohann for the use of FGM data (provided under the lead of the Technical University of Braunschweig and with financial support through the German Ministry for Economy and Technology and the German Center for Aviation and Space (DLR) under Contract 50 OC 0302). The work of X. J. Z. was also supported by RBSP-EMFISIS and RBSP-ECT funding 443956-TH-81074 and 443956-TH-79425 under NASA's prime Contract NNN06AA01C. We gratefully acknowledge Van Allen Probes EMFISIS data obtained through online website (https://emfisis.physics.uiowa.edu/data/index), THEMIS data from online website (http://themis.ssl.berkeley.edu/), Demeter IDP and ICE data available from the CNES/CESR Centre de Donnees pour la Physique des Plasmas (CDPP, France; https://cdpp-archive.cnes.fr/), GOES data from online website (https://satdat.ngdc.noaa.gov/sem/goes/data/full/), and POES data from the NOAA (http://satdat.ngdc.noaa.gov/sem/poes/data/). Data access and processing was done using SPEDAS V3.1 (see Angelopoulos et al., 2019).

References

Agapitov, O. V., Mourenas, D., Artemyev, A. V., Mozer, F. S., Hospodarsky, G., Bonnell, J., & Krasnoselskikh, V. (2018). Synthetic empirical chorus wave model from combined Van Allen Probes and Cluster statistics. *Journal of Geophysical Research: Space Physics*, *123*, 297–314. https://doi.org/10.1002/2017JA024843

Albert, J. M., & Bortnik, J. (2009). Nonlinear interaction of radiation belt electrons with electromagnetic ion cyclotron waves. *Geophysical Research Letters*, *36*, 12110. https://doi.org/10.1029/2009GL038904

Angelopoulos, V. (2008). The THEMIS Mission. *Space Science Reviews*, *141*, 5–34. https://doi.org/10.1007/s11214-008-9336-1

Angelopoulos, V., Cruce, P., Drozdov, A., Grimes, E. W., Hatzigeorgiu, N., King, D. A., & Schroeder, P. (2019). The Space Physics Environment Data Analysis System (SPEDAS). *Space Science Reviews*, *215*, 9. https://doi.org/10.1007/s11214-018-0576-4

Angelopoulos, V., McFadden, J. P., Larson, D., Carlson, C. W., Mende, S. B., Frey, H., & Kepko, L. (2008). Tail reconnection triggering substorm onset. *Science*, *321*, 931–935. https://doi.org/10.1126/science.1160495

Artemyev, A. V., Vasiliev, A. A., Mourenas, D., Agapitov, O., Krasnoselskikh, V., Boscher, D., & Rolland, G. (2014). Fast transport of resonant electrons in phase space due to nonlinear trapping by whistler waves. *Geophysical Research Letters*, *41*, 5727–5733. https://doi.org/10.1002/2014GL061380

Auster, H. U., Glassmeier, K. H., Magnes, W., Aydogar, O., Baumjohann, W., Constantinescu, D., & Wiedemann, M. (2008). The THEMIS Fluxgate Magnetometer. *Space Science Reviews*, *141*, 235–264. https://doi.org/10.1007/s11214-008-9365-9

Blum, L. W., Bonnell, J. W., Agapitov, O., Paulson, K., & Kletzing, C. (2017). EMIC wave scale size in the inner magnetosphere: Observations from the dual Van Allen Probes. *Geophysical Research Letters*, *44*, 1227–1233. https://doi.org/10.1002/2016GL072316

Blum, L. W., Halford, A., Millan, R., Bonnell, J. W., Goldstein, J., Usanova, M., & Li, X. (2015). Observations of coincident EMIC wave activity and duskside energetic electron precipitation on 18–19 January 2013. *Geophysical Research Letters*, *42*, 5727–5735. https://doi.org/10.1002/2015GL065245

Bonnell, J. W., Mozer, F. S., Delory, G. T., Hull, A. J., Ergun, R. E., Cully, C. M., & Harvey, P. R. (2008). The Electric Field Instrument (EFI) for THEMIS. *Space Science Reviews*, *141*, 303–341. https://doi.org/10.1007/s11214-008-9469-2

Bortnik, J., Inan, U. S., & Bell, T. F. (2006). Landau damping and resultant unidirectional propagation of chorus waves. *Geophysical Research Letters*, *33*, 3102. https://doi.org/10.1029/2005GL024553

Boynton, R. J., Mourenas, D., & Balikhin, M. A. (2016). Electron flux dropouts at Geostationary Earth Orbit: Occurrences, magnitudes, and main driving factors. *Journal of Geophysical Research: Space Physics*, *121*, 8448–8461. https://doi.org/10.1002/2016JA022916

Boynton, R. J., Mourenas, D., & Balikhin, M. A. (2017). Electron flux dropouts at $L \sim 4.2$ from Global Positioning System Satellites: Occurrences, magnitudes, and main driving factors. *Journal of Geophysical Research: Space Physics*, *122*, 11,428–11,441. https://doi.org/10.1002/2017JA024523

Cao, J., Shprits, Y. Y., Ni, B., & Zhelavskaya, I. S. (2017). Scattering of ultra-relativistic electrons in the Van Allen Radiation Belts accounting for hot plasma effects. *Scientific Reports*, *7*, 17719. https://doi.org/10.1038/s41598-017-17739-7

Capannolo, L., Li, W., Ma, Q., Zhang, X. J., Redmon, R. J., Rodriguez, J. V., & Reeves, G. D. (2018). Understanding the driver of energetic electron precipitation using coordinated multisatellite measurements. *Geophysical Research Letters*, *45*, 6755–6765. https://doi.org/10.1029/2018GL078604

Chen, L., & Hasegawa, A. (1991). Kinetic theory of geomagnetic pulsations. I—Internal excitations by energetic particles. *Journal of Geophysical Research*, *96*, 1503–1512. https://doi.org/10.1029/90JA02346

Chen, L., Thorne, R. M., Bortnik, J., & Zhang, X. J. (2016). Nonresonant interactions of electromagnetic ion cyclotron waves with relativistic electrons. *Journal of Geophysical Research: Space Physics*, *121*, 9913–9925. https://doi.org/10.1002/2016JA022813

Chen, L., Thorne, R. M., Jordanova, V. K., Thomsen, M. F., & Horne, R. B. (2011). Magnetosonic wave instability analysis for proton ring distributions observed by the LANL magnetospheric plasma analyzer. *Journal of Geophysical Research*, *116*, 3223. https://doi.org/10.1029/2010JA016068

Degeling, A. W., Ozeke, L. G., Rankin, R., Mann, I. R., & Kabin, K. (2008). Drift resonant generation of peaked relativistic electron distributions by Pc 5 ULF waves. *Journal of Geophysical Research*, *113*, A02208. https://doi.org/10.1029/2007JA012411

Green, J. C., Onsager, T. G., O'Brien, T. P., & Baker, D. N. (2004). Testing loss mechanisms capable of rapidly depleting relativistic electron flux in the Earth's outer radiation belt. *Journal of Geophysical Research*, *109*, A12211. https://doi.org/10.1029/2004JA010579

Hartinger, M. D., Turner, D. L., Plaschke, F., Angelopoulos, V., & Singer, H. (2013). The role of transient ion foreshock phenomena in driving Pc5 ULF wave activity. *Journal of Geophysical Research: Space Physics*, *118*, 299–312. https://doi.org/10.1029/2012JA018349

Hendry, A. T., Rodger, C. J., & Clilverd, M. A. (2017). Evidence of sub-MeV EMIC-driven electron precipitation. *Geophysical Research Letters*, *44*, 1210–1218. https://doi.org/10.1002/2016GL071807

Kang, S. B., Min, K. W., Fok, M. C., Hwang, J., & Choi, C. R. (2015). Estimation of pitch angle diffusion rates and precipitation time scales of electrons due to EMIC waves in a realistic field model. *Journal of Geophysical Research: Space Physics*, *120*, 8529–8546. https://doi.org/10.1002/2014JA020644

Kepko, L., & Spence, H. E. (2003). Observations of discrete, global magnetospheric oscillations directly driven by solar wind density variations. *Journal of Geophysical Research*, *108*(A6), 1257. https://doi.org/10.1029/2002JA009676

Kersten, T., Horne, R. B., Glauert, S. A., Meredith, N. P., Fraser, B. J., & Grew, R. S. (2014). Electron losses from the radiation belts caused by EMIC waves. *Journal of Geophysical Research: Space Physics*, *119*, 8820–8837. https://doi.org/10.1002/2014JA020366

Kivelson, M. G., & Southwood, D. J. (1986). Coupling of global magnetospheric MHD eigenmodes to field line resonances. *Journal of Geophysical Research*, *91*, 4345–4351. https://doi.org/10.1029/JA091iA04p04345

Kletzing, C. A., Kurth, W. S., Acuna, M., MacDowall, R. J., Torbert, R. B., Averkamp, T., & Tyler, J. (2013). The Electric and Magnetic Field Instrument Suite and Integrated Science (EMFISIS) on RBSP. *Space Science Reviews*, *179*, 127–181. https://doi.org/10.1007/s11214-013-9993-6

Kurth, W. S., De Pascuale, S., Faden, J. B., Kletzing, C. A., Hospodarsky, G. B., Thaller, S., & Wygant, J. R. (2015). Electron densities inferred from plasma wave spectra obtained by the waves instrument on Van Allen Probes. *Journal of Geophysical Research: Space Physics*, *120*, 904–914. https://doi.org/10.1002/2014JA020857

Lee, D. Y., Shin, D. K., Kim, J. H., Cho, J. H., Kim, K. C., Hwang, J. A., & Park, M. Y. (2013). Long-term loss and re-formation of the outer radiation belt. *Journal of Geophysical Research: Space Physics*, *118*, 3297–3313. https://doi.org/10.1002/jgra.50357

Li, J., Bortnik, J., Li, W., Thorne, R. M., Ma, Q., Chu, X., & Thaller, S. (2017). Coherently modulated whistler mode waves simultaneously observed over unexpectedly large spatial scales. *Journal of Geophysical Research: Space Physics*, *122*, 1871–1882. https://doi.org/10.1002/2016JA023706

Li, W., Thorne, R. M., Bortnik, J., Nishimura, Y., & Angelopoulos, V. (2011). Modulation of whistler mode chorus waves: 1. Role of compressional Pc4–5 pulsations. *Journal of Geophysical Research*, *116*, A06205. https://doi.org/10.1029/2010JA016312

Mathie, R. A., & Mann, I. R. (2001). On the solar wind control of Pc5 ULF pulsation power at mid-latitudes: Implications for MeV electron acceleration in the outer radiation belt. *Journal of Geophysical Research*, *106*, 29783–29796. https://doi.org/10.1029/2001JA000002

Mauk, B. H., Fox, N. J., Kanekal, S. G., Kessel, R. L., Sibeck, D. G., & Ukhorskiy, A. (2013). Science objectives and rationale for the Radiation Belt Storm Probes Mission. *Space Science Reviews*, *179*, 3–27. https://doi.org/10.1007/s11214-012-9908-y

Menk, F. W. (2011). *Magnetospheric ULF waves: A review*. Netherlands, Dordrecht: Springer. https://doi.org/10.1007/978-94-007-0501-2

Meredith, N. P., Horne, R. B., Kersten, T., Fraser, B. J., & Grew, R. S. (2014). Global morphology and spectral properties of EMIC waves derived from CRRES observations. *Journal of Geophysical Research: Space Physics*, *119*, 5328–5342. https://doi.org/10.1002/2014JA020064

Mourenas, D., Artemyev, A. V., Ma, Q., Agapitov, O. V., & Li, W. (2016). Fast dropouts of multi-MeV electrons due to combined effects of EMIC and whistler mode waves. *Geophysical Research Letters*, *43*, 4155–4163. https://doi.org/10.1002/2016GL068921

Mourenas, D., Ma, Q., Artemyev, A. V., & Li, W. (2017). Scaling laws for the inner structure of the radiation belts. *Geophysical Research Letters*, *44*, 3009–3018. https://doi.org/10.1002/2017GL072987

Murphy, K. R., Mann, I. R., Rae, I. J., Sibeck, D. G., & Watt, C. E. J. (2016). Accurately characterizing the importance of wave-particle interactions in radiation belt dynamics: The pitfalls of statistical wave representations. *Journal of Geophysical Research: Space Physics*, *121*, 7895–7899. https://doi.org/10.1002/2016JA022618

Mursula, K., Bräysy, T., Niskala, K., & Russell, C. T. (2001). Pc1 pearls revisited: Structured electromagnetic ion cyclotron waves on Polar satellite and on ground. *Journal of Geophysical Research*, *106*, 29543–29554. https://doi.org/10.1029/2000JA003044

Ni, B., Cao, X., Shprits, Y. Y., Summers, D., Gu, X., Fu, S., & Lou, Y. (2018). Hot plasma effects on the cyclotron-resonant pitch-angle scattering rates of radiation belt electrons due to EMIC waves. *Geophysical Research Letters*, *45*, 21–30. https://doi.org/10.1002/2017GL076028

Omura, Y., & Zhao, Q. (2013). Relativistic electron microbursts due to nonlinear pitch angle scattering by EMIC triggered emissions. *Journal of Geophysical Research: Space Physics*, *118*, 5008–5020. https://doi.org/10.1002/jgra.50477

Ozeke, L. G., Mann, I. R., Murphy, K. R., Rae, I. J., & Milling, D. K. (2014). Analytic expressions for ULF wave radiation belt radial diffusion coefficients. *Planatary Space Science*, *119*, 1587–1605. https://doi.org/10.1002/2013JA019204

Parrot, M., Benoist, D., Berthelier, J. J., Błęcki, J., Chapuis, Y., Colin, F., & Zamora, P. (2006). The magnetic field experiment IMSC and its data processing onboard DEMETER: Scientific objectives, description and first results. *Planatary Space Science*, *54*, 441–455. https://doi.org/10.1016/j.pss.2005.10.015

Potapov, A., Guglielmi, A., Tsegmed, B., & Kultima, J. (2006). Global Pc5 event during 29–31 October 2003 magnetic storm. *Advances in Space Research*, *38*, 1582–1586. https://doi.org/10.1016/j.asr.2006.05.010

Rae, I. J., Murphy, K. R., Watt, C. E. J., Halford, A. J., Mann, I. R., Ozeke, L. G., & Singer, H. J. (2018). The role of localized compressional ultra-low frequency waves in energetic electron precipitation. *Journal of Geophysical Research: Space Physics*, *123*, 1900–1914. https://doi.org/10.1002/2017JA024674

Remya, B., Sibeck, D. G., Halford, A. J., Murphy, K. R., Reeves, G. D., Singer, H. J., & Thaller, S. A. (2018). Ion injection triggered EMIC waves in the Earth's magnetosphere. *Journal of Geophysical Research: Space Physics*, *123*, 4921–4938. https://doi.org/10.1029/2018JA025354

Runov, A., Angelopoulos, V., Sitnov, M. I., Sergeev, V. A., Bonnell, J., McFadden, J. P., & Auster, U. (2009). THEMIS observations of an earthward-propagating dipolarization front. *Geophysical Research Letters*, *36*, L14106. https://doi.org/10.1029/2009GL038980

Runov, A., Sergeev, V. A., Angelopoulos, V., Glassmeier, K. H., & Singer, H. J. (2014). Diamagnetic oscillations ahead of stopped dipolarization fronts. *Journal of Geophysical Research: Space Physics*, *119*, 1643–1657. https://doi.org/10.1002/2013JA019384

Sandanger, M., Søraas, F., Aarsnes, K., Oksavik, K., & Evans, D. S. (2007). Loss of relativistic electrons: Evidence for pitch angle scattering by electromagnetic ion cyclotron waves excited by unstable ring current protons. *Journal of Geophysical Research*, *112*, A12213. https://doi.org/10.1029/2006JA012138

Sauvaud, J. A., Moreau, T., Maggiolo, R., Treilhou, J. P., Jacquey, C., Cros, A., & Gangloff, M. (2006). High-energy electron detection onboard DEMETER: The IDP spectrometer, description and first results on the inner belt. *Planatary Space Science*, *54*, 502–511. https://doi.org/10.1016/j.pss.2005.10.019

Shprits, Y. Y., Thorne, R. M., Horne, R. B., & Summers, D. (2006). Bounce-averaged diffusion coefficients for field-aligned chorus waves. *Journal of Geophysical Research*, *111*, 10225. https://doi.org/10.1029/2006JA011725

Simms, L. E., Engebretson, M. J., Clilverd, M. A., Rodger, C. J., & Reeves, G. D. (2018). Nonlinear and synergistic effects of ULF Pc5, VLF chorus, and EMIC waves on relativistic electron flux at geosynchronous orbit. *Journal of Geophysical Research: Space Physics*, *123*, 4755–4766. https://doi.org/10.1029/2017JA025003

Su, Y. J., Johnston, W. R., Albert, J. M., Ginet, G. P., Starks, M. J., & Roth, C. J. (2012). SCATHA measurements of electron decay times at $5 < L < 8$. *Journal of Geophysical Research*, *117*, 8212. https://doi.org/10.1029/2012JA017685

Summers, D., & Thorne, R. M. (2003). Relativistic electron pitch-angle scattering by electromagnetic ion cyclotron waves during geomagnetic storms. *Journal of Geophysical Research*, *108*(A4), 1143. https://doi.org/10.1029/2002JA009489

Thorne, R. M., & Kennel, C. F. (1971). Relativistic electron precipitation during magnetic storm main phase. *Journal of Geophysical Research*, *76*, 4446. https://doi.org/10.1029/JA076i019p04446

Turner, D. L., Shprits, Y., Hartinger, M., & Angelopoulos, V. (2012). Explaining sudden losses of outer radiation belt electrons during geomagnetic storms. *Nature Physics*, *8*, 208–212. https://doi.org/10.1038/nphys2185

Usanova, M. E., Drozdov, A., Orlova, K., Mann, I. R., Shprits, Y., Robertson, M. T., & Wygant, J. (2014). Effect of EMIC waves on relativistic and ultrarelativistic electron populations: Ground-based and Van Allen Probes observations. *Geophysical Research Letters*, *41*, 1375–1381. https://doi.org/10.1002/2013GL059024

Wang, G., Su, Z., Zheng, H., Wang, Y., Zhang, M., & Wang, S. (2017). Nonlinear fundamental and harmonic cyclotron resonant scattering of radiation belt ultrarelativistic electrons by oblique monochromatic EMIC waves. *Journal of Geophysical Research: Space Physics*, *122*, 1928–1945. https://doi.org/10.1002/2016JA023451

Wang, C. P., Xing, X., Nakamura, T. K. M., Lyons, L. R., & Angelopoulos, V. (2014). Source and structure of bursty hot electron enhancements in the tail magnetosheath: Simultaneous two-probe observation by ARTEMIS. *Journal of Geophysical Research: Space Physics*, *119*, 9900–9918. https://doi.org/10.1002/2014JA020603

Wygant, J. R., Bonnell, J. W., Goetz, K., Ergun, R. E., Mozer, F. S., Bale, S. D., & Tao, J. B. (2013). The electric field and waves instruments on the Radiation Belt Storm Probes Mission. *Space Science Reviews*, *179*, 183–220. https://doi.org/10.1007/s11214-013-0013-7

Xia, Z., Chen, L., Dai, L., Claudepierre, S. G., Chan, A. A., Soto-Chavez, A. R., & Reeves, G. D. (2016). Modulation of chorus intensity by ULF waves deep in the inner magnetosphere. *Geophysical Research Letters*, *43*, 9444–9452. https://doi.org/10.1002/2016GL070280

Xiang, Z., Tu, W., Ni, B., Henderson, M. G., & Cao, X. (2018). A statistical survey of radiation belt dropouts observed by Van Allen Probes. *Geophysical Research Letters*, *45*, 8035–8043. https://doi.org/10.1029/2018GL078907

Yu, J., Li, L. Y., Cao, J. B., Yuan, Z. G., Reeves, G. D., Baker, D. N., & Spence, H. (2015). Multiple loss processes of relativistic electrons outside the heart of outer radiation belt during a storm sudden commencement. *Journal of Geophysical Research: Space Physics*, *120*, 10. https://doi.org/10.1002/2015JA021460

Zhang, X. J., Li, W., Thorne, R. M., Angelopoulos, V., Bortnik, J., Kletzing, C. A., & Hospodarsky, G. B. (2016). Statistical distribution of EMIC wave spectra: Observations from Van Allen Probes. *Geophysical Research Letters*, *43*, 12. https://doi.org/10.1002/2016GL071158

Zhang, X. J., Mourenas, D., Artemyev, A. V., Angelopoulos, V., & Thorne, R. M. (2017). Contemporaneous EMIC and whistler mode waves: Observations and consequences for MeV electron loss. *Geophysical Research Letters*, *44*, 8113–8121. https://doi.org/10.1002/2017GL073886